RESEARCH ARTICLE | SEPTEMBER 17 2025

In-plane thermal conductivity and the applicability of the Wiedemann–Franz law in dilute AlCu thin films

Sara Makarem ; Shivashree Gowda; Ramya Mohan; Saman Zare ; Md. Nazmun Sadat Khan ; Ian A. Brummel ; Chung T. Ma ; Md. Shafkat Bin Hoque; Daniel Hirt ; Md. Rafiqul Islam; Joseph Poon ; Jon F. Ihlefeld ; Giovanni Esteves ; Ethan A. Scott ; Patrick E. Hopkins

Appl. Phys. Lett. 127, 112204 (2025)
https://doi.org/10.1063/5.0284972
CHORUS

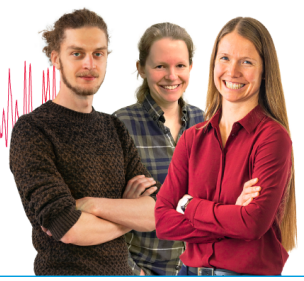

Applied Physics Letters ARTICLE pubs.aip.org/aip/apl

In-plane thermal conductivity and the applicability of the Wiedemann–Franz law in dilute AlCu thin films

Cite as: Appl. Phys. Lett. **127**, 112204 (2025); doi: 10.1063/5.0284972
Submitted: 11 June 2025 · Accepted: 23 August 2025 ·
Published Online: 17 September 2025

View Online Export Citation CrossMark

Sara Makarem,[1] Shivashree Gowda,[2] Ramya Mohan,[2,a)] Saman Zare,[2] Md. Nazmun Sadat Khan,[3] Ian A. Brummel,[1] Chung T. Ma,[3] Md. Shafkat Bin Hoque,[2] Daniel Hirt,[2] Md. Rafiqul Islam,[2] Joseph Poon,[1,4] Jon F. Ihlefeld,[1,4] Giovanni Esteves,[5] Ethan A. Scott,[2] and Patrick E. Hopkins[1,2,3,b)]

AFFILIATIONS

[1]Department of Materials Science and Engineering, University of Virginia, Charlottesville, Virginia 22904, USA
[2]Department of Mechanical and Aerospace Engineering, University of Virginia, Charlottesville, Virginia 22904, USA
[3]Department of Physics, University of Virginia, Charlottesville, Virginia 22904, USA
[4]Charles L. Brown Department of Electrical and Computer Engineering, University of Virginia, Charlottesville, Virginia 22904, USA
[5]Microsystems Engineering, Science and Applications (MESA), Sandia National Laboratories, Albuquerque, New Mexico 87123, USA

[a)]**Current address:** Oshani Labs Pvt. Ltd., Margao – 403601, Goa, India
[b)]**Author to whom correspondence should be addressed:** phopkins@virginia.edu

ABSTRACT

The Wiedemann–Franz (WF) law correlates heat and charge transport in metals. However, the validity of this correlation remains an open-ended question, especially in the context of inelastic scattering at room temperature. To address this gap in knowledge, we perform independent measurements of the in-plane thermal and electrical conductivities across four AlCu (0.5% Cu) films [thickness (h) ≈ 174, 98, 53, and 24 nm] using optical pump–probe metrologies and four-point probe techniques, respectively. For in-plane thermal conductivity measurements, we utilize time-domain thermoreflectance, in both concentric and beam-offset configurations, and the time-resolved magneto-optic Kerr effect. Our results show that the WF law overpredicts the thermal conductivity by at least ∼10% in all films, thus demonstrating modest deviations in predicted thermal conductivity when applying the WF law to dilute AlCu films. Using infrared variable angle spectroscopic ellipsometry, we demonstrate increased electron scattering rates in the thinnest film ($h \approx 24$ nm), indicating electron-boundary scattering drives the reduction in in-plane thermal conductivity. This is generally an elastic scattering process, which is supported by our thermal conductivity measurements and analysis.

Dilute aluminum copper (AlCu, ∼0.5 wt. % Cu, (111)-textured) is an important metal-templating film used to deposit highly textured aluminum nitride (AlN) and aluminum scandium nitride (AlScN).[1] Well-textured AlN films are widely employed in high electron mobility transistors, ultraviolet light-emitting diodes, and high-power radio frequency devices due to their high thermal conductivity, optical transparency, and favorable piezoelectric properties.[2–6] Alloying AlN with scandium not only enhances its piezoelectric response but also induces ferroelectric behavior.[7–9] The use of a metallic AlCu underlayer can enable higher Sc incorporation in AlScN, further improving its piezoelectric and ferroelectric performance,[1] while also serving as a potential bottom electrode to support ferroelectric device integration. Therefore, dilute AlCu thin films are critical from a device engineering standpoint, and a comprehensive understanding of their microstructure–thermal property relationships is essential for next generation device design. Such insights will aid in effective thermal management, thereby enhancing device reliability and operational lifetime.

Building upon the critical role of dilute AlCu thin films in device engineering, it is essential to consider the implications of miniaturization on their thermal properties.[10–12] As devices continue to shrink in size, the thickness and grain size of AlCu films approach length scales comparable to the electronic mean free path. This proximity introduces significant size effects that influence heat transport phenomena. In metallic films, heat conduction is predominantly mediated by electrons. Consequently, to quantify thermal conductivity in metallic

systems such as the AlCu films studied in this work, the traditional approach has been to perform four-point probe electrical resistivity measurements and apply the WF law. However, as film dimensions decrease and size effects become pronounced, the WF law fails to accurately predict thermal conductivity.[13–16]

According to the Wiedemann–Franz law, the ratio of electronic thermal conductivity to electrical conductivity in metals is proportional to temperature, with the proportionality constant, known as the Lorenz number, assumed to take the Sommerfeld value, $L_0 = 2.44 \times 10^{-8}\,\mathrm{W\,\Omega\,K^{-2}}$.[17] When phonon contributions are negligible, this law allows thermal conductivity to be estimated from the more easily measurable electrical conductivity.[17] It also provides a means to distinguish electron and phonon contributions when the total thermal conductivity is known.[18,19] However, its applicability in metallic nanostructures is debated. Some researchers have reported Lorenz numbers larger than the Sommerfeld value,[18,20–23] while others have found values comparable to or lower than L_0.[14,24–28] Additionally, it remains unclear whether the Lorenz number exhibits size and temperature dependence.[13,24,29] Thus, the WF law cannot always be reliably used to characterize thermal transport in sub-micrometer metallic films, necessitating independent in-plane thermal conductivity measurements using methods that are not reliant on electrical resistivity.

In this work, our primary goal is to uniquely characterize the in-plane thermal and electrical transport in four polycrystalline AlCu films of varying thicknesses and evaluate the applicability of the WF law under conditions of reduced film dimensionality. Three of the films have thicknesses considerably larger than the electronic mean free path of Al ($\mathrm{MFP_{Al}} \approx 19$ nm, Ref. 30) with thicknesses $h \approx 174$, 98, and 53 nm, whereas the fourth film with a thickness of $h \approx 24$ nm has physical dimensions comparable to the $\mathrm{MFP_{Al}}$.[30]

To measure the in-plane thermal conductivity, we utilize two optical pump–probe metrologies: time-domain thermoreflectance (TDTR), in both concentric and beam-offset configurations, and the time-resolved magneto-optic Kerr effect (TR-MOKE). Electrical conductivity is determined using the four-point probe method. Our results show that the WF law overpredicts the thermal conductivity by at least ~10% in all films, thus demonstrating modest deviations in predicted thermal conductivity when applying the WF law to dilute AlCu films. Using infrared variable angle spectroscopic ellipsometry (IR-VASE), we demonstrate increased electron scattering rates in the thinnest film ($h \approx 24$ nm), indicating electron-boundary scattering drives the reduction in in-plane thermal conductivity. This is generally an elastic scattering process, which is supported by our thermal conductivity measurements and analysis.

All AlCu films were deposited onto silicon wafers coated with a 1.5 μm amorphous SiO_2 layer via physical vapor deposition (PVD); detailed deposition conditions are provided in Ref. 1. The resulting stack geometry, top down, consists of AlCu film/SiO_2 (1.5 μm)/silicon, as illustrated in the schematic in Fig. 1(a). The purpose of coating the Si substrate with a thick insulating oxide layer is to maximize the sensitivity to the in-plane thermal conductivity in the AlCu film, with minimal influence from the background substrate conductance. Film

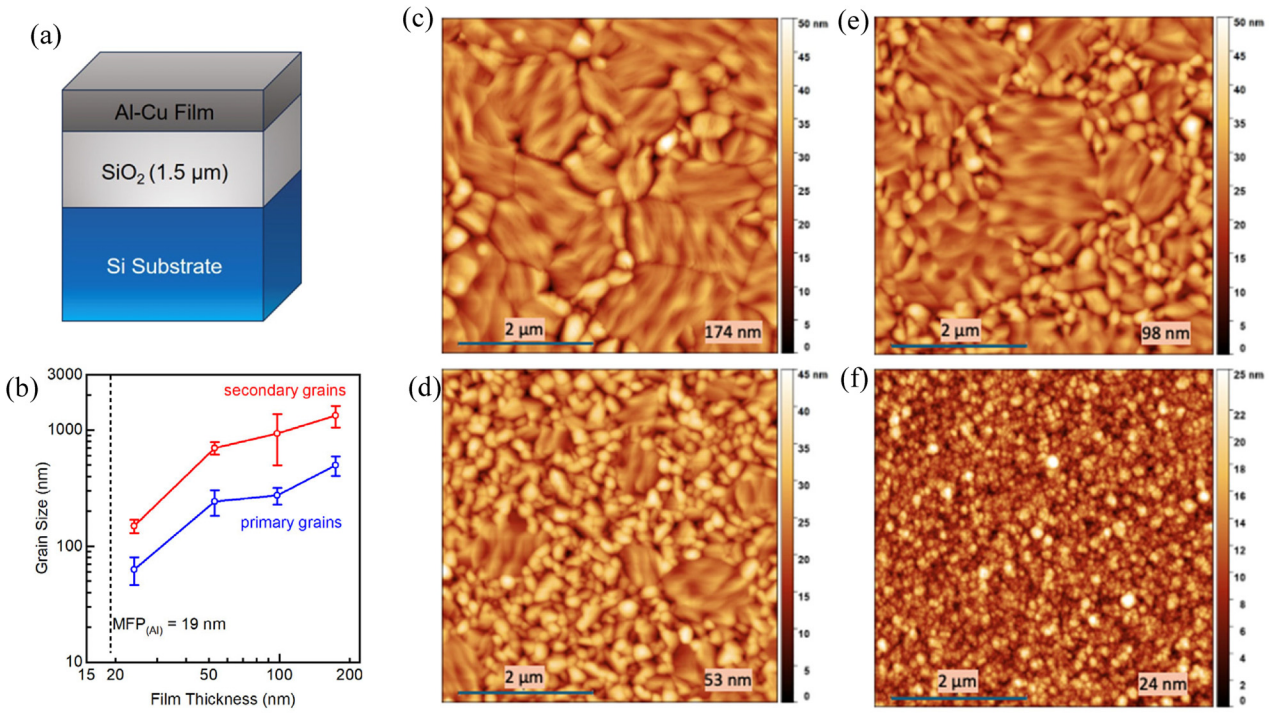

FIG. 1. AlCu film characterization. (a) A schematic depicting the AlCu sample stack is shown. (b) Grain sizes (both secondary and primary grains) are plotted as a function of AlCu film thickness; the Al mean free path, $\mathrm{MFP_{Al}} = 19$ nm, is indicated by a dashed black line. Grain sizes were measured using ImageJ processing of atomic force microscopy (AFM) images; representative micrographs for all four films are shown in panels (c)–(f). All films show a bimodal grain distribution, with smaller primary and larger secondary grains.

thicknesses were determined using x-ray reflectometry (XRR). To characterize the grain size distribution, topographic atomic force microscopy (AFM) was performed in alternating current (AC) mode. Representative surface micrographs are shown in Figs. 1(c)–1(f). Grain sizes were quantified using ImageJ. A summary of the grain size measurements and analysis is provided in supplementary material note 1.

As shown in Figs. 1(c)–1(f), all of our AlCu films exhibit a bimodal grain distribution; that is, larger secondary grains surrounded by smaller primary grains. In Fig. 1(b), we plot grain size as a function of film thickness and show that both primary and secondary grains exhibit a near-linear increase in size with increasing film thickness beyond 53 nm, and we observe a sharp drop in grain size in the ∼24 nm AlCu film. Additionally, x-ray diffraction (XRD) was employed to characterize the crystallographic texture of the AlCu films. Films with thicknesses $\geq$ 53 nm exhibit a predominant (111) orientation, whereas the 24 nm film does not display the same texturing. However, given the isotropic nature of thermal transport in AlCu alloys, variations in crystallographic texture are not expected to significantly influence the measured in-plane thermal conductivity in this film. The corresponding diffractograms are provided in supplementary material note 1. Following these characterizations, we perform four-point probe measurements of electrical resistivity at room temperature. The details of this measurement are provided in supplementary material note 7.

We measure the in-plane thermal conductivity of all four AlCu films using time-domain thermoreflectance (TDTR), a well-established optical pump–probe technique for thermal property measurements in both bulk and thin-film systems.[31,32] Additional details are provided in supplementary material note 2. In our TDTR experiment, we directly pump and probe the AlCu films without depositing an additional transducer layer, as illustrated in the schematic in Fig. 2(a). This approach maximizes sensitivity to the in-plane thermal conductivity (κ_r). To reliably measure κ_r, the radial thermal conductance in the AlCu film, given by $\kappa_r \times h$, where h is the film thickness, must exceed the conductance of any deposited transducer film.[33] A typical TDTR experiment employs a high thermal conductance ∼80 nm Al transducer film; however, depositing Al transducer

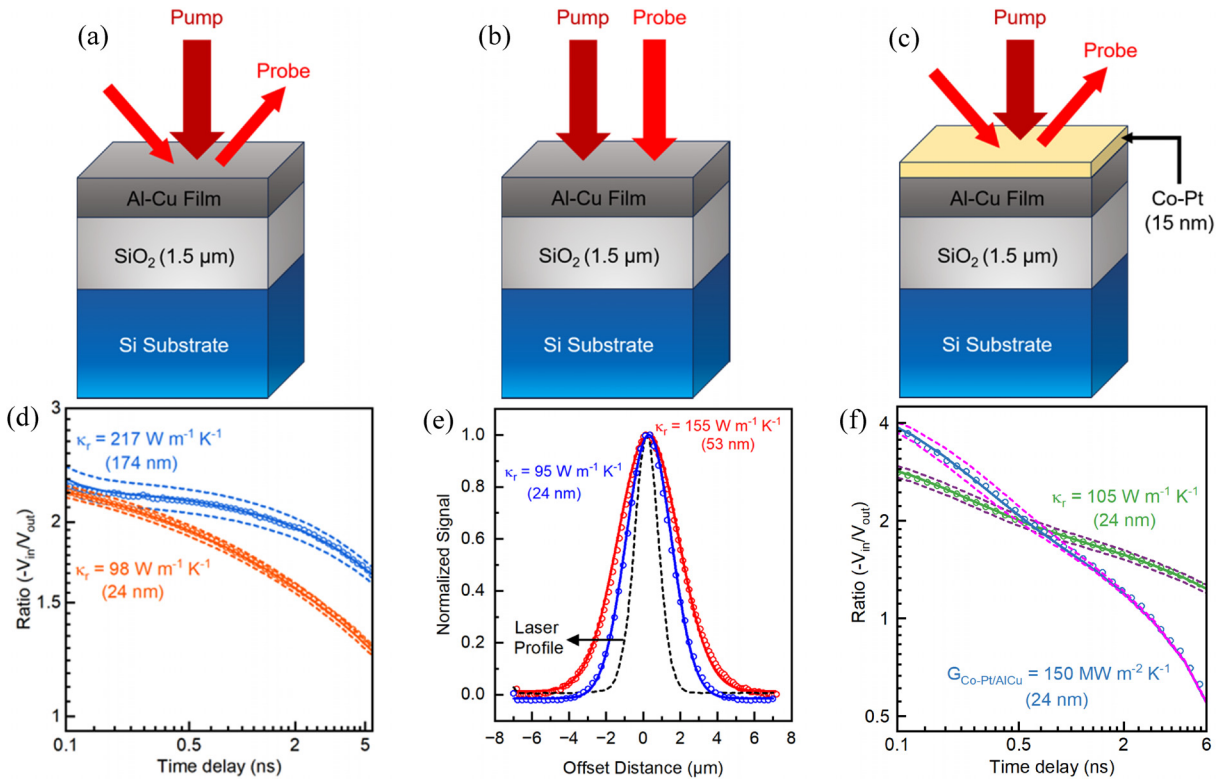

FIG. 2. AlCu thin-film thermal conductivity measurements. Schematics showing the sample geometry and pump–probe configurations for (a) transducer-less concentric TDTR, (b) pump beam-offset TDTR, and (c) TR-MOKE measurements using a Co-Pt transducer, are provided. Representative datasets for each measurement technique are shown below the schematic. (d) For a concentric TDTR measurement performed at $f_{mod} = 1.1$ MHz and $\omega_0 = 2.51$ μm, the ratio between the in-phase and out-of-phase signals ($-V_{in}/V_{out}$) is plotted as a function of pump–probe time delay. We fit for the in-plane thermal conductivity of the AlCu film (κ_r) in both the thickest (i.e., 174 nm) and the thinnest (i.e., 24 nm) films. The dashed lines represent a 10% perturbation in κ_r. (e) For a pump beam-offset TDTR measurement, the normalized V_{out} signal, collected as a function of pump offset distance, at a time delay of -100 ps, is shown for the 53 nm (in red) and 24 nm (in blue) films. The FWHM of the resultant Gaussian signal intensity is fit with the thermal model to determine κ_r. We provide a direct demonstration of the lateral in-plane heat spreading in both the films at $f_{mod} = 1.1$ MHz and $\omega_0 = 1.67$ μm. The black dashed lines are indicative of the laser beam profile collected at $f_{mod} = 8.4$ MHz at a time delay of +100 ps (i.e., $1/e^2$ Gaussian spot size). (f) A dual-frequency variable-spot size MOKE measurement performed at $f_{mod} = 8.4$ MHz and $\omega_0 = 5.1$ μm (indicated in blue, where $G_{Co-Pt/AlCu}$ is the fitting parameter) and $f_{mod} = 1.1$ MHz and $\omega_0 = 2.3$ μm (indicated in green, where κ_r is the fitting parameter) is shown for the 24 nm AlCu film. The dashed lines in both cases represent a 15% perturbation in G and a 10% perturbation in κ_r.

significantly reduces sensitivity to the κ_r of the underlying AlCu films, particularly for the thinner films, 53 and 24 nm (see additional discussion in supplementary material note 2 for more detailed information). Therefore, to accurately resolve κ_r, we perform transducer-less TDTR measurements, which are further enabled by the high optical opacity and favorable signal-to-noise ratio (SNR) of the metallic AlCu films.

Another requisite condition for measuring κ_r is that the thermal penetration depth (d_p) in the AlCu film, given by $d_p = \sqrt{\frac{\kappa}{\pi C f_{mod}}}$, where C is the volumetric heat capacity, must be larger than the $1/e^2$ radius of the focused laser spot (ω_0) on the sample surface; that is, $d_p > \omega_0$.[34] The choice of pump modulation frequency directly dictates the thermal penetration depth.

Accordingly, our measurements were performed at a modulation frequency of approximately 1.1 MHz with spot sizes ranging from $\omega_0 \approx 2.4$–$2.5\ \mu$m, thus providing high sensitivity to the radial thermal conductivity (κ_r) across all four AlCu films. We determine the spot size for each film individually, as detailed in Table I. Figure 2(d) presents representative TDTR datasets, showing the signal ratio as a function of pump–probe time delay, where we uniquely fit for κ_r using the thermal model, reporting values of 217 W m^{-1} K^{-1} for the thickest film (174 nm) and 98 W m^{-1} K^{-1} for the thinnest film (24 nm).

We also consider the thermal boundary conductance (G) between the AlCu film and the SiO_2 layer. The measurement sensitivity to G depends on the thermal mass of the AlCu film, given by $h \times C$. To accurately measure G, the thickness of the AlCu film must be comparable to the Kapitza length at the AlCu/SiO_2 interface (L_K), defined as $L_K \approx \kappa_{SiO_2}/G$.[35] Considering the reported G values in the literature for metal–amorphous dielectric interfaces ($\approx$200–500 MW m^{-2} K^{-1})[35,36] and κ_{SiO_2}=1.25 W m^{-1} K^{-1}, we compute $L_K \approx 2.5$–6.5 nm, which is significantly smaller than the thickness of all four AlCu films measured in our work. Hence, we are unable to reliably resolve and report G across any of the AlCu/SiO_2 interfaces. However, we note a non-negligible sensitivity to G in the 24 nm AlCu film (see discussion in supplementary material note 2), which contributes to the uncertainty in our measured κ_r values. Therefore, to independently measure κ_r in the thinnest AlCu films with minimal sensitivity to cross-plane thermal conductances (such as G and the cross-plane thermal conductivity, κ_z, in the sample stack layers), we perform pump–probe beam-offset TDTR measurements for the AlCu films with $h \approx 53$ and 24 nm.[33,37]

TABLE I. Spot sizes and thermal penetration depths for sensitivity to κ_r at $f_{mod} = 1.1$ MHz. In-plane thermal conductivity (κ_r) values reported in this table are measured using concentric TDTR. The spot size for each measurement was determined using a pump beam-offset scan, where the normalized V_{in} signal was collected at $f_{mod} \approx 8.4$ MHz at a time delay of +100 ps and fit to a Gaussian profile (see supplementary material Note 5 for more information). The thermal penetration depth ($d_p = \sqrt{\kappa/(\pi C f_{mod})}$) was calculated for each film using $f_{mod} = 1.1$ MHz and $C = 2.42$ MJ m^{-3} K^{-1}.[38]

AlCu film thickness (nm)	In-plane thermal conductivity (W m^{-1} K^{-1})	Spot size (μm)	Thermal penetration depth (μm)
174	212 ± 17	2.51	5.03
98	185 ± 10	2.49	4.70
53	150 ± 20	2.43	4.23
24	98 ± 21	2.43	3.42

Figure 2(b) presents a schematic of the beam-offset TDTR configuration, where the pump beam is steered across a stationary probe beam. The resulting convoluted pump–probe V_{out} signal is recorded as a function of the lateral offset distance at a fixed delay time of −100 ps and a modulation frequency of 1.1 MHz; this configuration, in conjunction with a $1/e^2$ spot radius of $\omega_0 \approx 1.67\ \mu$m, renders the heat transport three-dimensional, as the thermal penetration depth exceeds the laser spot size ($d_p > \omega_0$). This enhances the sensitivity to the in-plane thermal conductivity (κ_r) in the AlCu films. As shown in Fig. 2(e), the normalized V_{out} signals for the 53 nm (red) and 24 nm (blue) films reveal a broader lateral heat spread in the 53 nm film, consistent with its higher in-plane thermal conductivity.

To obtain κ_r, we fit the full width at half maximum (FWHM) of the normalized V_{out} signal to the thermal model described by Feser *et al.* in Ref. 37. We report κ_r values of 155 W m^{-1} K^{-1} for the 53 nm film and 95 W m^{-1} K^{-1} for the 24 nm film, both of which are in excellent agreement with the values obtained from concentric TDTR measurements. Additionally, we plot the Gaussian laser beam profile, indicated by the dashed black line, which corresponds to the V_{in} signal acquired at $f_{mod} \approx 8.4$ MHz and a time delay of +100 ps. Further experimental details are provided in supplementary material note 3.

Finally, for the optically semi-transparent 24 nm AlCu film, we consider the possibility of non-negligible signal artifacts arising from the optical absorbance of the underlying SiO_2/Si substrate, which could potentially skew the reported κ_r value from TDTR experiments. This concern arises because the $1/e^2$ optical penetration depth of Al is approximately 39 nm at a wavelength of ~800 nm,[39] which is larger than the thickness of the 24 nm AlCu film. To address this issue, we perform a TR-MOKE measurement on the 24 nm AlCu film after depositing a ~16 nm Co-Pt magnetic transducer layer, as illustrated in the schematic in Fig. 2(c). TR-MOKE is a technique analogous to TDTR, with the key difference being that, instead of probing a thermoreflectance response, it probes the thermo-magnetic response of the Co-Pt transducer upon pump-induced heating.[36,40,41] Thus, the V_{in} and V_{out} signals obtained in a TR-MOKE measurement depend solely on the magnetization of the transducer film, and any non-magnetic signal from the underlying stack layers is canceled out (see supplementary material note 4 for additional details). Furthermore, the radial thermal conductance in a 16 nm Co–Pt transducer ($\kappa \approx 16$ W m^{-1} K^{-1}) is ~0.24 μW K^{-1}, an order of magnitude lower than the conductance in the AlCu film, at ~2.4 μW K^{-1}, making our measurement extremely sensitive to κ_r.

We design our TR-MOKE experiment to account for the two unknown thermal parameters in our sample stack: κ_r of the AlCu film and G at the Co-Pt/AlCu interface. To uniquely determine both parameters, we utilize a dual-frequency, variable-spot size approach,[34,42] wherein we perform two measurements, as shown in Fig. 2(f). The first measurement, represented by the red dataset, is conducted at a high modulation frequency ($f_{mod} \approx 8.4$ MHz) and a large spot size ($\omega_0 \approx 5.1\ \mu$m), where the heat flux is one-dimensional, and the signal ratio exhibits enhanced sensitivity to G with no sensitivity to κ_r. We, therefore, fit solely for G and report a value of 150 MW m^{-2} K^{-1}.

The second measurement, depicted by the green dataset, is performed at a lower modulation frequency ($f_{mod} \approx 1.1$ MHz) and a smaller spot size ($\omega_0 \approx 2.3\ \mu$m), where the heat flux becomes

three-dimensional, and the ratio is sensitive to both G and κ_r. In this case, we fix G to the previously determined value and fit for κ_r, reporting a value of 105 W m^{-1} K^{-1}. This value is approximately 10% higher than that obtained using TDTR. While the two values agree reasonably well within the bounds of experimental uncertainty, we use the κ_r value obtained from TR-MOKE for the remainder of this work. For additional details on the TR-MOKE methodology, refer to supplementary material note 4.

It is worth noting that at low modulation frequencies, such as those used in this study, both TDTR and TR-MOKE measurements are highly sensitive to the laser spot size.[31] Therefore, we adopt a three-pronged approach to rigorously characterize the spot size for each measurement, ensuring a deviation of no more than 2%, as detailed in supplementary material note 5.

In Fig. 3(a), we plot a summary of the measured in-plane electronic thermal conductivity (κ_e), as derived from the WF law applied to our four-point probe measurements of electrical resistivity, and the in-plane thermal conductivities (κ_r) as measured via our thermoreflectance techniques described above. We first examine κ_e: in all our thicker films (174, 98, and 53 nm), we show that κ_e is consistent within a 10% deviation, and in reasonable agreement with thermal conductivity of bulk Al at 237 W m^{-1} K^{-1}.[38] This suggests that dilute alloying of Al with Cu (0.5%) does not significantly affect electronic transport, and thus, any alloy-based scattering of electrons is minimal. In the 24 nm film, we show a precipitous drop in κ_e by ~50%, to a value of 119 ± 5 W m^{-1} K^{-1}, likely due to inelastic electron scattering at the film boundaries. While grain boundary scattering may contribute to some extent, our data suggest that it is not the dominant mechanism limiting the in-plane thermal conductivity in our AlCu films. This conclusion is supported by our grain size analysis presented in Fig. 1(b) and supplementary material note 1. Even in the thinnest film (24 nm), the primary grain size is approximately three times larger than the electron mean free path in Al (Al_{MFP}), while the secondary grain size has a mean value of ~150 nm, well above the Al_{MFP}. As the film thickness increases, the grain sizes grow significantly, reaching several hundred nanometers. Despite this grain size increase, we observe that κ_e is fairly consistent and within agreement with the Al bulk value for the three thicker films, indicating that film thickness, not grain size, is the primary driver of the observed size effects.

Next, we turn to κ_r, which exhibits a monotonically decreasing gradient with decreasing film thickness, with an equally sharp drop in the 24 nm film, again possibly due to interfacial scattering of electrons in the film. In Fig. 3(b), we assess the applicability of the WF law by comparing the electronic thermal conductivity (κ_e) with the measured radial thermal conductivity (κ_r), using the relation $\kappa_r = \kappa_e L_0 T$, where L_0 is the Sommerfeld value of the Lorenz number and T is room temperature (300 K). Using the standard value $L_0 = 2.44 \times 10^{-8}$ W Ω K^{-2}, we observe clear deviations from the WF law across all four AlCu films. However, when the data are fitted using an effective Lorenz number, $L_{eff} = 2.14 \times 10^{-8}$ W Ω K^{-2} (blue solid line), we find good agreement between κ_e and κ_r in the 174, 98, and 24 nm films. A comparable ~10%–30% reduction in L_{eff} was also reported by Mason *et al.*[13] for Au films with comparable thicknesses at 300 K, supporting the consistency of our findings.

The strongest deviation from the WF law is observed in the 53 nm AlCu film, where $\kappa_e \approx \kappa_r$ only when using a significantly reduced $L_{eff} = 1.65 \times 10^{-8}$ W Ω K^{-2} (see green solid line). We tentatively attribute this pronounced violation to enhanced phonon scattering resulting from intrinsic structural anisotropy in the 53 nm film. During deposition of textured microcrystalline films onto amorphous substrates, initial grain growth forms circular morphologies, termed the "nucleation layer." Beyond this layer, grains adopt a columnar

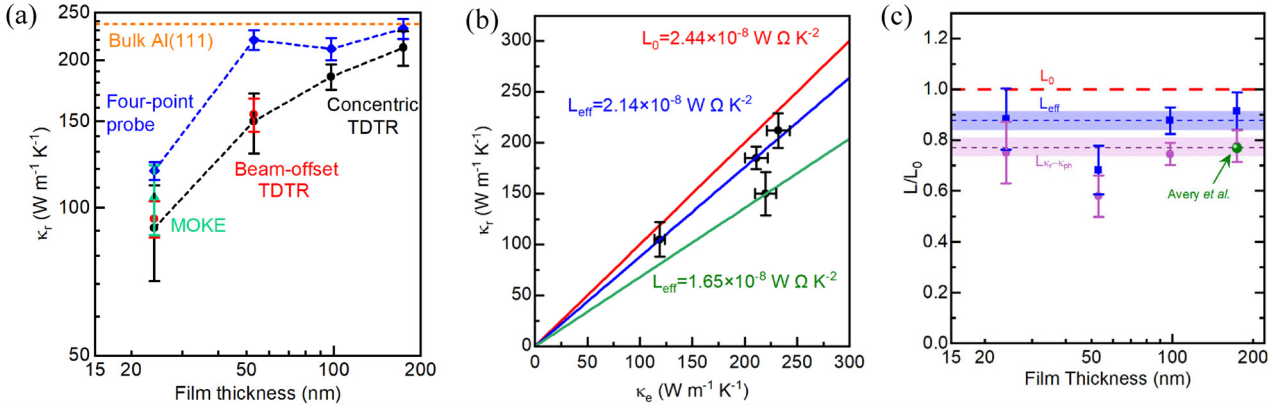

FIG. 3. AlCu thermal conductivities and the applicability of the WF law. (a) A summary of the in-plane thermal conductivities (κ_r) obtained using concentric TDTR (black solid circles) for all films, beam-offset TDTR (red solid circles) for the 53 and 24 nm films, and TR-MOKE (green solid triangle) for the 24 nm film are plotted vs AlCu film thicknesses. Electrical thermal conductivities (κ_e) obtained using four-probe (blue solid diamonds), and thermal conductivity of bulk Al (dashed orange line) are also shown. κ_r exhibits a monotonically decreasing gradient with decreasing film thickness, whereas κ_e is fairly consistent (and within agreement with bulk Al values) until film dimensions approach the MFP_{Al} in the thinnest film. Note: dashed lines are guidelines between data points and are not model fits. (b) κ_r vs κ_e with model calculations from $\kappa_r = \kappa_e L_0 T$ (the WF law, solid lines). Assuming the Sommerfeld–Lorenz number, $L_0 = 2.44 \times 10^{-8}$ W Ω K^{-2} does not yield good fits for any of our films. However, a 12% lower "effective Lorenz number," $L_{eff} = 2.14 \times 10^{-8}$ W Ω K^{-2} provides a good fit for the 174, 98, and 24 nm films, whereas a 32% lower $L_{eff} = 1.65 \times 10^{-8}$ W Ω K^{-2} provides a good fit for the 53 nm film. Thus, we experimentally demonstrate violations in the WF law for all our measured AlCu films.(c) Lorenz number of AlCu thin films as a function of thickness. The electronic component of the thermal conductivity is estimated as ($\kappa_r - \kappa_{ph}$), where κ_{ph} for Al is taken from Ref. 43 to be 15% of κ_r. The Sommerfeld value L_0 (dashed red), the effective Lorenz number L_{eff} from direct measurements (dashed blue), and the Lorenz number calculated after subtracting phonon contribution, $L_{(\kappa_r - \kappa_{ph})}$, (dashed purple) are shown. $L_{(\kappa_r - \kappa_{ph})}$ is in close alignment with the reported value at room temperature in Ref. 14.

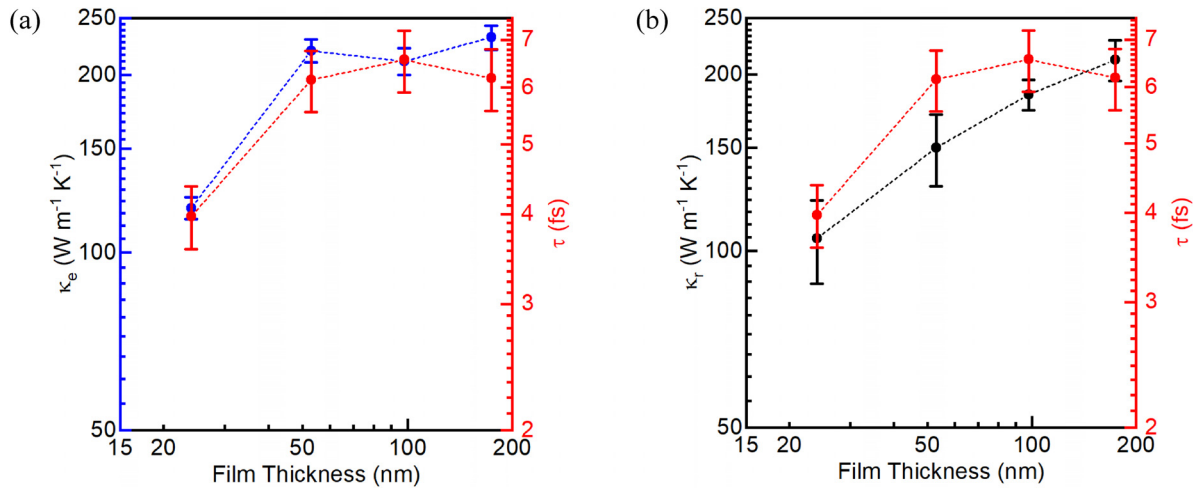

FIG. 4. Film thickness effects on in-plane thermal conductivity in AlCu thin films. We correlate (a) κ_e (as derived from the WF law) and (b) κ_r with electron relaxation lifetimes (τ), measured using IR-VASE, in all our films. We show that τ scales proportionately with κ_e in all four films.

structure, introducing anisotropy that may scatter heat carriers (phonons) more strongly than charge carriers (electrons), thus leading to a stronger breakdown of the WF law. We conjecture that this morphological transition from circular to columnar grains initiates near the 53 nm thickness. A comparable violation of the WF law due to structural anisotropy has also been reported by Mason *et al.*[13] in their experimental study of κ_e and κ_r in Au thin films.

Prior studies have shown that the lattice (phonon) contribution, κ_{ph}, to the total in-plane thermal conductivity, κ_r, of metal thin films such as aluminum, gold, and silver is generally small, typically accounting for no more than ~15% of the overall heat transport.[43] For example, in copper, the contribution of the lattice thermal conductivity is ~7%.[12] This indicates that heat conduction in these metallic systems is predominantly governed by electronic carriers. Building on this understanding, we estimate the Lorenz number for our AlCu films by isolating the electronic portion of the thermal conductivity, i.e., $(\kappa_r - \kappa_{ph})$, where the phonon contribution, κ_{ph}, is taken from literature values for aluminum thin films (Ref. 43) to be 15% of the κ_r. Figure 3(c) presents a comparison between the Sommerfeld value L_0 (dashed red line), the effective Lorenz number L_{eff} derived directly from our measurements (dashed blue line), and the Lorenz number calculated after subtracting the phonon contribution, $L_{(\kappa_r - \kappa_{ph})}$ (dashed purple line). The results demonstrate strong alignment with a previously reported Lorenz number for a 174 nm aluminum thin film at room temperature.[14]

To investigate the origins of the observed discrepancy in the WF law, we extract electronic scattering rates for all AlCu films using infrared variable angle spectroscopic ellipsometry (IR-VASE) assuming a Drude model. The inverse of these scattering rates yields the electron relaxation time (τ) (see supplementary material note 6 for further details). In Fig. 4(a), we plot κ_e and τ as a function of film thickness, demonstrating a direct correlation in the trends of κ_e and τ across all thicknesses. However, as shown in Fig. 4(b) τ and κ_r do not follow this same agreement for the 53 nm film, with this deviation between τ and κ_r beginning for the 98 nm film, albeit minor and within the outer bounds of uncertainty. While we cannot currently point to the origin of this statistically significant deviation for the 53 nm film, we note that the measured thermal conductivity for this film deviates from the WF law predictions by ~30%. For the thinnest and thickest films, we find generally good agreement between the measured in-plane thermal conductivity, those predicted by the WF law (within ~10%) and the measured electron scattering rates, implying that elastic electronic scattering processes are contributing to electron thermal conductivity. This slight deviation from the WF law calculations for these thin and thick films could be due to some combination of inelastic electron–phonon scattering and phonon thermal transport. The larger deviation between κ_r and both the WF law-derived κ_e and τ at the 53 and 98 nm film thicknesses could indicate an increased inelastic scattering mechanism for electrons that is significant for these moderate film thicknesses. For the thinnest film, as this approaches the electron mean free path in Al, the thermal transport is likely dominated by elastic electron-boundary scattering events, thus leading to realignment among τ, κ_r, and κ_e.

In conclusion, we have independently measured the thermal and electrical conductivities of four AlCu films with varying thicknesses and demonstrated that the WF law overpredicts κ_r in all cases. While this overprediction is relatively minor and within the bounds of uncertainty in the thinnest and thickest cases, for moderate film thicknesses, this deviation is as much as 30%. Our IR-VASE analysis supports that for the thinnest film, where the film thickness approaches the electron mean free path in Al, elastic electron scattering events from film boundaries are driving the reduction in in-plane thermal conductivity.

See the supplementary material for a comprehensive account of the film characterization, including full details of the thermoreflectance measurements, ellipsometry analyses, and electrical resistivity assessments.

Optical and electrical characterization were supported by the Semiconductor Research Corporation, Grant No. 2025-NM-3286.

Conceptualization, thermal characterization, and interpretation were supported as part of the Center for 3D Ferroelectric Microelectronics Manufacturing, an Energy Frontier Research Center funded by the U.S. Department of Energy, Office of Science, Basic Energy Sciences under Award No. DE-SC0021118. Film growth and characterization were supported under Contract No. DE-NA0003525 at Sandia National Laboratories, a multimission laboratory managed and operated by National Technology and Engineering Solutions of Sandia, LLC, a wholly owned subsidiary of Honeywell International Inc., for the U.S. Department of Energy's National Nuclear Security Administration. This paper describes objective technical results and analysis. Any subjective views or opinions that might be expressed in the paper do not necessarily represent the views of the U.S. Department of Energy or the United States Government. This article has been authored by an employee of National Technology & Engineering Solutions of Sandia, LLC under Contract No. DE-NA0003525 with the U.S. Department of Energy (DOE). The employee owns all right, title and interest in and to the article and is solely responsible for its contents. The United States Government retains and the publisher, by accepting the article for publication, acknowledges that the United States Government retains a non-exclusive, paid-up, irrevocable, world-wide license to publish or reproduce the published form of this article or allow others to do so, for United States Government purposes. The DOE will provide public access to these results of federally sponsored research in accordance with the DOE Public Access Plan https://www.energy.gov/downloads/doe-public-access-plan.

AUTHOR DECLARATIONS

Conflict of Interest

The authors have no conflicts to disclose.

Author Contributions

Sara Makarem: Conceptualization (equal); Data curation (equal); Formal analysis (equal); Project administration (equal); Validation (equal); Writing – original draft (equal); Writing – review & editing (equal). **Shivashree Gowda:** Data curation (equal). **Ramya Mohan:** Data curation (equal); Formal analysis (equal); Validation (equal); Writing – review & editing (equal). **Saman Zare:** Data curation (equal); Formal analysis (equal); Writing – review & editing (equal). **Md. Nazmun Sadat Khan:** Data curation (equal). **Ian A. Brummel:** Data curation (equal); Formal analysis (equal). **Chung T. Ma:** Resources (equal). **Md. Shafkat Bin Hoque:** Writing – review & editing (equal). **Daniel Hirt:** Conceptualization (equal). **Md. Rafiqul Islam:** Conceptualization (equal). **Joseph Poon:** Conceptualization (supporting); Resources (equal). **Jon F. Ihlefeld:** Conceptualization (supporting); Investigation (equal); Resources (equal); Supervision (equal); Visualization (equal); Writing – review & editing (equal). **Giovanni Esteves:** Resources (equal); Writing – review & editing (equal). **Ethan A. Scott:** Conceptualization (equal); Supervision (supporting); Writing – review & editing (equal). **Patrick E. Hopkins:** Conceptualization (equal); Funding acquisition (equal); Resources (equal); Supervision (equal); Validation (equal); Writing – review & editing (equal).

DATA AVAILABILITY

The data that support the findings of this study are available from the corresponding author upon reasonable request.

REFERENCES

[1]G. Esteves, M. Berg, K. D. Wrasman, M. David Henry, B. A. Griffin, and E. A. Douglas, "CMOS compatible metal stacks for suppression of secondary grains in $Sc_{0.125}Al_{0.875}N$," J. Vac. Sci. Technol. A **37**(2), 021511 (2019).
[2]F. Miyashiro, N. Iwase, A. Tsuge, F. Ueno, M. Nakahashi, and T. Takahashi, "High thermal conductivity aluminum nitride ceramic substrates and packages," IEEE Trans. Compon., Hybrids, Manuf. Technol. **13**, 313–319 (1990).
[3]L. Lindsay, D. A. Broido, and T. L. Reinecke, "*Ab initio* thermal transport in compound semiconductors," Phys. Rev. B **87**(16), 165201 (2013).
[4]M. S. Bin Hoque, Y. R. Koh, J. L. Braun, A. Mamun, Z. Liu, K. Huynh, M. E. Liao, K. Hussain, Z. Cheng, E. R. Hoglund, D. H. Olson, J. A. Tomko, K. Aryana, R. Galib, J. T. Gaskins, M. M. M. Elahi, Z. C. Leseman, J. M. Howe, T. Luo, S. Graham, M. S. Goorsky, A. Khan, and P. E. Hopkins, "High in-plane thermal conductivity of aluminum nitride thin films," ACS Nano **15**(6), 9588–9599 (2021).
[5]Y. Lu, M. Reusch, N. Kurz, A. Ding, T. Christoph, M. Prescher, L. Kirste, O. Ambacher, and A. Žukauskaitė, "Elastic modulus and coefficient of thermal expansion of piezoelectric $Al_{1-x}Sc_xN$ (up to $x = 0.41$) thin films," APL Mater. **6**(7), 076105 (2018).
[6]J. Y. Tsao, S. Chowdhury, M. A. Hollis, D. Jena, N. M. Johnson, K. A. Jones, R. J. Kaplar, S. Rajan, C. G. Van de Walle, E. Bellotti, C. L. Chua, R. Collazo, M. E. Coltrin, J. A. Cooper, K. R. Evans, S. Graham, T. A. Grotjohn, E. R. Heller, M. Higashiwaki, M. S. Islam, P. W. Juodawlkis, M. A. Khan, A. D. Koehler, J. H. Leach, U. K. Mishra, R. J. Nemanich, R. C. N. Pilawa-Podgurski, J. B. Shealy, Z. Sitar, M. J. Tadjer, A. F. Witulski, M. Wraback, and J. A. Simmons, "Ultrawide-bandgap semiconductors: Research opportunities and challenges," Adv. Elect. Mater. **4**(1), 1600501 (2018).
[7]S. Fichtner, N. Wolff, F. Lofink, L. Kienle, and B. Wagner, "AlScN: A III-V semiconductor based ferroelectric," J. Appl. Phys. **125**(11), 114103 (2019).
[8]N. Wolff, S. Fichtner, B. Haas, M. R. Islam, F. Niekiel, M. Kessel, O. Ambacher, C. Koch, B. Wagner, F. Lofink, and L. Kienle, "Atomic scale confirmation of ferroelectric polarization inversion in wurtzite-type AlScN," J. Appl. Phys. **129**(3), 034103 (2021).
[9]W. Sui, H. Wang, J. Lee, A. Qamar, M. Rais-Zadeh, and P. X. L. Feng, "AlScN-on-SiC thin film micromachined resonant transducers operating in high-temperature environment up to 600 °C," Adv. Funct. Mater. **32**(34), 2202204 (2022).
[10]R. Cheaito, "The role of size effects on the thermal conductivity of thin film alloys and superlattices approval sheet," Ph.D. dissertation (University of Virginia, 2015).
[11]J. L. Braun, C. H. Baker, A. Giri, M. Elahi, K. Artyushkova, T. E. Beechem, P. M. Norris, Z. C. Leseman, J. T. Gaskins, and P. E. Hopkins, "Size effects on the thermal conductivity of amorphous silicon thin films," Phys. Rev. B **93**, 140201 (2016).
[12]M. R. Islam, P. Karna, J. A. Tomko, E. R. Hoglund, D. M. Hirt, M. S. Bin Hoque, S. Zare, K. Aryana, T. W. Pfeifer, C. Jezewski, A. Giri, C. D. Landon, S. W. King, and P. E. Hopkins, "Evaluating size effects on the thermal conductivity and electron-phonon scattering rates of copper thin films for experimental validation of Matthiessen's rule," Nat. Commun. **15**(1), 9167 (2024).
[13]S. J. Mason, D. J. Wesenberg, A. Hojem, M. Manno, C. Leighton, and B. L. Zink, "Violation of the Wiedemann-Franz law through reduction of thermal conductivity in gold thin films," Phys. Rev. Mater. **4**(6), 065003 (2020).
[14]A. D. Avery, S. J. Mason, D. Bassett, D. Wesenberg, and B. L. Zink, "Thermal and electrical conductivity of approximately 100-nm permalloy, Ni, Co, Al, and Cu films and examination of the Wiedemann-Franz Law," Phys. Rev. B **92**(21), 214410 (2015).
[15]M. Islam, P. Karna, N. Bhatt, S. Thakur, H. Heinrich, D. M. Hirt, S. Zare, C. Jezewski, R. T. P. Lee, K. Tapily, J. T. Gaskins, C. D. Landon, S. W. King, A. Giri, and P. E. Hopkins, "Unveiling phonon contributions to thermal transport and the failure of the Wiedemann-Franz Law in ruthenium and tungsten thin films," arXiv:2505.07613 (2025).
[16]H. Yi, J. Y. Kim, H. Z. Gul, S. Kang, G. Kim, E. Sim, H. Ji, J. Kim, Y. C. Choi, W. S. Kim, and S. C. Lim, "Wiedemann-Franz law of Cu-coated carbon fiber," Carbon **162**, 339–345 (2020).

[17]G. V. Chester and A. Thellung, "The Law of Wiedemann and Franz," Proc. Phys. Soc. **77**, 1005–1013 (1961).
[18]W. Ma and X. Zhang, "Study of the thermal, electrical and thermoelectric properties of metallic nanofilms," Int. J. Heat Mass Transfer **58**(1–2), 639–651 (2013).
[19]B. L. Zink, A. D. Avery, R. Sultan, D. Bassett, and M. R. Pufall, "Exploring thermoelectric effects and Wiedemann-Franz violation in magnetic nanostructures via micromachined thermal platforms," Solid State Commun. **150**(11–12), 514–518 (2010).
[20]H. Wang, J. Liu, X. Zhang, and K. Takahashi, "Breakdown of Wiedemann-Franz law in individual suspended polycrystalline gold nanofilms down to 3 K," Int. J. Heat Mass Transfer **66**, 585–591 (2013).
[21]H. Lin, S. Xu, C. Li, H. Dong, and X. Wang, "Thermal and electrical conduction in 6.4 nm thin gold films," Nanoscale **5**(11), 4652–4656 (2013).
[22]Z. Cheng, L. Liu, S. Xu, M. Lu, and X. Wang, "Temperature dependence of electrical and thermal conduction in single silver nanowire," Sci. Rep. **5**, 10718 (2015).
[23]X. Zhang, H. Xie, M. Fujii, H. Ago, K. Takahashi, T. Ikuta, H. Abe, and T. Shimizu, "Thermal and electrical conductivity of a suspended platinum nanofilm," Appl. Phys. Lett. **86**(17), 171912 (2005).
[24]S. D. Sawtelle and M. A. Reed, "Temperature-dependent thermal conductivity and suppressed Lorenz number in ultrathin gold nanowires," Phys. Rev. B **99**(5), 054304 (2019).
[25]D. Kojda, R. Mitdank, M. Handwerg, A. Mogilatenko, M. Albrecht, Z. Wang, J. Ruhhammer, M. Kroener, P. Woias, and S. F. Fischer, "Temperature-dependent thermoelectric properties of individual silver nanowires," Phys. Rev. B **91**(2), 024302 (2015).
[26]Y. Zhao, M. L. Fitzgerald, Y. Tao, Z. Pan, G. Sauti, D. Xu, Y. Q. Xu, and D. Li, "Electrical and thermal transport through silver nanowires and their contacts: Effects of elastic stiffening," Nano Lett. **20**(10), 7389–7396 (2020).
[27]J. Wang, Z. Wu, C. Mao, Y. Zhao, J. Yang, and Y. Chen, "Effect of electrical contact resistance on measurement of thermal conductivity and Wiedemann-Franz law for individual metallic nanowires," Sci. Rep. **8**(1), 4862 (2018).
[28]J. Wang, H. Yu, T. Walbert, M. Antoni, C. Wang, W. Xi, F. Muench, J. Yang, Y. Chen, and W. Ensinger, "Electrical and thermal conductivities of polycrystalline platinum nanowires," Nanotechnology **30**(45), 455706 (2019).
[29]F. Völklein, H. Reith, T. W. Cornelius, M. Rauber, and R. Neumann, "The experimental investigation of thermal conductivity and the Wiedemann-Franz law for single metallic nanowires," Nanotechnology **20**(32), 325706 (2009).
[30]D. Gall, "Electron mean free path in elemental metals," J. Appl. Phys. **119**(8), 085101 (2016).
[31]D. G. Cahill, "Analysis of heat flow in layered structures for time-domain thermoreflectance," Rev. Sci. Instrum. **75**(12), 5119–5122 (2004).
[32]P. Jiang, X. Qian, and R. Yang, "Tutorial: Time-domain thermoreflectance (TDTR) for thermal property characterization of bulk and thin film materials," J. Appl. Phys. **124**(16), 161103 (2018).
[33]J. P. Feser, J. Liu, and D. G. Cahill, "Pump-probe measurements of the thermal conductivity tensor for materials lacking in-plane symmetry," Rev. Sci. Instrum. **85**(10), 104903 (2014).
[34]P. Jiang, X. Qian, and R. Yang, "Time-domain thermoreflectance (TDTR) measurements of anisotropic thermal conductivity using a variable spot size approach," Rev. Sci. Instrum. **88**(7), 074901 (2017).
[35]J. Kimling, A. Philippi-Kobs, J. Jacobsohn, H. P. Oepen, and D. G. Cahill, "Thermal conductance of interfaces with amorphous SiO_2 measured by time-resolved magneto-optic Kerr-effect thermometry," Phys. Rev. B **95**(18), 184305 (2017).
[36]J. Liu, G. M. Choi, and D. G. Cahill, "Measurement of the anisotropic thermal conductivity of molybdenum disulfide by the time-resolved magneto-optic Kerr effect," J. Appl. Phys. **116**(23), 233107 (2014).
[37]J. P. Feser and D. G. Cahill, "Probing anisotropic heat transport using time-domain thermoreflectance with offset laser spots," Rev. Sci. Instrum. **83**(10), 104901 (2012).
[38]X. Zheng, D. G. Cahill, P. Krasnochtchekov, R. S. Averback, and J. C. Zhao, "High-throughput thermal conductivity measurements of nickel solid solutions and the applicability of the Wiedemann-Franz law," Acta Mater. **55**(15), 5177–5185 (2007).
[39]A. J. Schmidt "Optical characterization of thermal transport from the nanoscale to the macroscale," Ph. D. thesis (Massachusetts Institute of Technology, 2008).
[40]J. Y. Chen, J. Zhu, D. Zhang, D. M. Lattery, M. Li, J. P. Wang, and X. Wang, "Time-resolved magneto-optical Kerr effect of magnetic thin films for ultrafast thermal characterization," J. Phys. Chem. Lett. **7**(13), 2328–2332 (2016).
[41]D. M. Lattery, J. Zhu, D. Huang, and X. Wang, "Ultrafast thermal and magnetic characterization of materials enabled by the time-resolved magneto-optical Kerr effect," in *Nanoscale Energy Transport* (IOP Publishing, 2020).
[42]X. Qian, P. Jiang, and R. Yang, "Anisotropic thermal conductivity of 4H and 6H silicon carbide measured using time-domain thermoreflectance," Mater. Today Phys. **3**, 70–75 (2017).
[43]A. Jain and A. J. H. McGaughey, "Thermal transport by phonons and electrons in aluminum, silver, and gold from first principles," Phys. Rev. B **93**(8), 081206 (2016).